Single-layer terahertz metamaterials with bulk optical constants

W.-C. Chen, A. Totachawattana, K. Fan, J. L. Ponsetto, A. C. Strikwerda, X. Zhang, R. D. Averitt, and W. J. Padilla

Phys. Rev. B **85**, 035112 — Published 17 January 2012

DOI: 10.1103/PhysRevB.85.035112

Single Layer Terahertz Metamaterials with Bulk Optical Constants

W. - C. Chen[1], A. Totachawattana[1], K. Fan[2], J. L. Ponsetto[1], A. C. Strikwerda[3], X. Zhang[2], R. D. Averitt[3], and W. J. Padilla[1]

[1]*Department of Physics, Boston College, 140 Commonwealth Ave., Chestnut Hill, MA 02467, USA*

[2]*Department of Mechanical Engineering, Boston University, 15 Saint Mary's St., Brookline, MA 02446, US and*

[3]*Department of Physics, Boston University, 590 Commonwealth Ave.,Boston, MA 02215 USA*

We investigate the conditions under which single layer metamaterials may be described by bulk optical constants. Terahertz time domain spectroscopy is utilized to investigate two types of geometries, both with two different sizes of embedding dielectric - cubic and tetragonal unit cells. The tetragonal metamaterials are shown to yield layer dependent optical constants, whereas the cubic metamaterials yielded layer independent optical constants. We establish guidelines for when ϵ and μ can be used as material parameters for single layer metamaterials. Experimental results at terahertz frequencies are presented and supported by full wave three dimensional electromagnetic simulations.

PACS numbers:

I. INTRODUCTION

Since the theoretical prediction[1] and experimental verification of[2–4] a negative refractive index, the field of electromagnetic metamaterials has experienced enormous growth. The unique properties of metamaterials create possibilities for novel applications difficult to achieve with naturally occurring materials - cloaking[5–7] and superlensing[8–10] being two prime examples. Although the aforementioned cases largely motivate metamaterials research, arguably the real power of metamaterials stems from their ability to construct materials with a specific electric and magnetic response. In practice this is achieved *via* two different metamaterial unit cells able to independently control the two parameters which govern light-matter interactions in Maxwell's equations - the electric permittivity (ϵ), and the magnetic permeability (μ).

The ability to assign optical constants (ϵ, μ) to materials greatly facilitates the description of the interaction of electromagnetic waves and matter. However this description is only possible when the wavelength (λ) is much greater than the element size (w), and distances between them (a), i.e. $\lambda \gg a > w$[11]. Compliance with these 'sub-wavelength' requirements ensures that electric and magnetic fields vary slowly over the individual elements and therefore experiences an averaged response. The particular microscopic details may thus be ignored and the electromagnetic response may be described as that being due to the optical constants of a homogeneous material in the so called "effective medium regime"[12].

However the optical constants are intimately connected to the density of electric and magnetic dipoles within a material. For example the definition of the electrical permittivity is $\epsilon = \epsilon_0(1 + \chi_e) = \epsilon_0\epsilon_r$, where ϵ_r is relative permittivity and the electric susceptibility χ_e describes the relation between the electric field (E) and the polarization (P), which is equal to the number of electric dipoles per unit volume, i.e. $P = p/V = \epsilon_0\chi_e E$, where p is the number of electric dipoles, V is the volume, and E is the electric field. A similar definition exists between the magnetic permeability $\mu = \mu_0(1+\chi_m) = \mu_0\mu_r$ and the magnetization (M), that is $M = m/V = \chi_m H$, where μ_r is relative permeability, m is the number of magnetic dipoles, χ_m is magnetic susceptibility, and H is the magnetic field. Metamaterials, on the other hand, obtain their electromagnetic response from a combination of their geometry and p and m. That is, metamaterial unit cells are well described as effective electric or magnetic dipoles and the true number of dipoles due to the constituent materials is, to first order, not relevant, so long as metamaterials are fashioned from highly conductive structures, and operated below the plasma frequency of the metal. Since it is the metamaterial unit cell that is the effective fundamental dipole one may, by extension, assume that metamaterials should be volumetric in order to appropriately describe their electromagnetic response by effective optical constants.

Metamaterials which extend significantly in three spatial directions are easily fabricated for operation at relatively low RF and microwave frequencies. These may be constructed using printed circuit board techniques thus permitting the assembly of bulk metamaterials. However at terahertz and higher frequencies it is typical to construct metamaterials consisting of a single layer on top of a substrate, owing to the relatively more complicated fabrication processes required - photo, electron beam, and/or focused ion beam lithography. Thus caution must be used when describing the optical constants of metamaterials at THz and higher frequencies as these structures do not significantly extend in a third dimension. As such, one must question the assignment of optical constants to all metamaterials which consist of a single or even of several layers.

There have been several works exploring the optical constants of single layer metamaterials[13–17], some of which term these structures "metasurfaces"[18–20]. Most works focus on obtaining ϵ and μ analytically and/or numerically, usually by direct inversion of the transfer ma-

trix equations. Regardless of whether a metamaterial consists of a single or multiple layers, the transfer matrix method permits electromagnetic scattering of a medium of thickness d to be described as[21,22],

$$t = \frac{1}{\cos(nkd) - \frac{i}{2}(Z_r + Z_r^{-1})\sin(nkd)} \tag{1}$$

$$r = -\frac{\frac{i}{2}(Z_r - Z_r^{-1})\sin(nkd)}{\cos(nkd) - \frac{i}{2}(Z_r + Z_r^{-1})\sin(nkd)} \tag{2}$$

where t is the transmission coefficient, r is the reflection coefficient, n is the index of refraction, Z_r is the relative impedance, and k is the wavevector. The refractive index is defined as $n = c/v$ and the impedance as $Z = Z_r Z_0 = E/H$, where c is the speed of light in vacuo, v is the velocity of light within the medium, Z is the impedance, Z_0 is the wave impedance of free space, E is the electric field, and H is the magnetic field. However in effective medium theory a connection may be made between the optical constants and the index of refraction and relative impedance, i.e. $n = \sqrt{\epsilon_r \mu_r}$ and $Z_r = \sqrt{\mu_r/\epsilon_r}$. Equations (1) may be inverted to yield explicit equations for the index of refraction and the impedance. We may then also connect these directly to the optical constants, i.e.

$$n = \frac{1}{kd}\arccos[\frac{1}{2t}(1 - (r^2 - t^2))] = \sqrt{\epsilon_r \mu_r} \tag{3}$$

$$Z_r = \sqrt{\frac{(1+r)^2 - t^2}{(1-r)^2 - t^2}} = \sqrt{\frac{\mu_r}{\epsilon_r}} \tag{4}$$

An outstanding question in metamaterials research is under what conditions the right side of Eqs. 3 and 4 are valid[23]. In this paper we investigate the cases under which single layer metamaterials may be described by the optical constants, thus satisfying Eqs. 3 and 4. Two different structures are studied, each with two different layer thicknesses, in order to demonstrate various prototypical results. A series of simulations and experiments are performed in order to clarify the dependence of the optical constants on metamaterial layer thickness.

II. DESIGN AND FABRICATION

We present two electric split ring resonator structures[24–27] in single and multilayer configurations, which we term ERR1 and ERR2, see Fig. 1. For both structures, the in-plane size of the unit cell is 50μm×50μm, and both the width and height of the metamaterial is 36μm, with a line width of 4μm. The capacitive gaps, found in the middle of the ERR2 structure and on the sides of the ERR1 structure, are 4μm. The metallic metamaterial layer is a 150nm thick layer of gold and is embedded (centered) within the substrate material, polyimide,

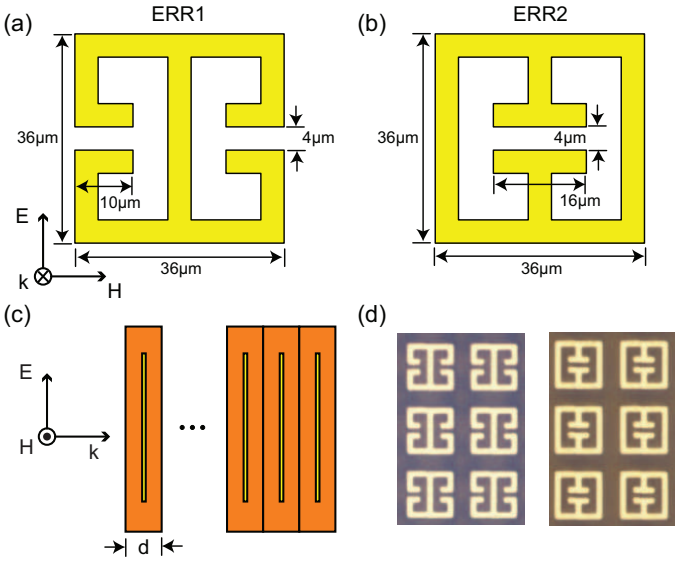

FIG. 1: Geometry and dimensions of (a) ERR1 and (b) ERR2. Polarization of the incident electromagnetic radiation is shown in (a) for both ERR1 and ERR2. A schematic detailing the stacking of multiple layers is shown in (c), along with the the incident polarization specified. Microscopic photographs of the fabricated samples are shown in (d).

giving a total unit cell thickness of either 50μm or 15μm , see Fig. 1. We term these two configurations as Type 50, and Type 15 based on their unit cell thickness. Each of these individual metamaterial unit cells (ERR1 and ERR2) of both substrate thicknesses (Type 50 and Type 15) are then stacked and we study n=1,2,3, and 4 layers of both structures and both types. Thus a total of sixteen different metamaterial samples are computationally and experimentally investigated.

Samples were fabricated with the dimensions shown in Fig. 1 (a) and (b) for ERR1 and ERR2, respectively. The structures were fabricated on layer-by-layer films of polyimide (PI-5878G HD Microsystems TM). Substrate thicknesses between adjacent metallic gold layers are chosen as mentioned above. Here we take the 50μm ERR1 as an example to demonstrate the fabrication process. First a 25μm layer of polyimide was spin coated on a silicon substrate and cured at 275°C in an N_2 environment for 5 hours. Then the 150nm thick gold metamaterial was fabricated and patterned using optical lithography and lift-off techniques. For better pattern transfer, vacuum contact mode was used during the exposure process.. Substrate thickness is accurate to $\pm$1μm. For samples with more than one layer, a second metamaterial layer was patterned in the same manner as the first. Alignment between the two layers was performed with a mask aligner which has an accuracy of 0.5μm. Additional layers of 50μm polyimide and 150nm gold can be coated and patterned in the same way. For the last layer, a 25μm thick layer of polyimide was coated on top. In the final

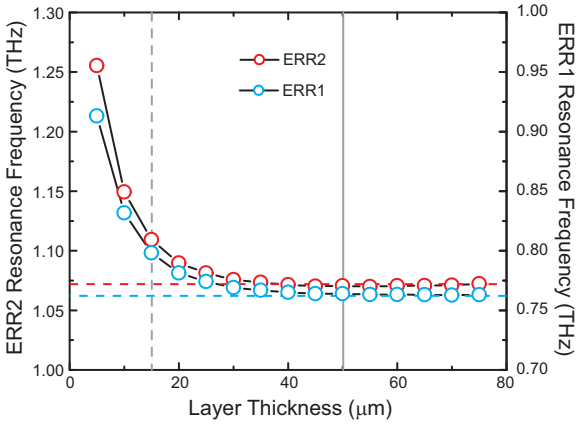

FIG. 2: Dependence of the resonant frequencies of ERR1 (blue symbols) and ERR2 (red symbols) (single layer structures) on the embedding substrate thickness.

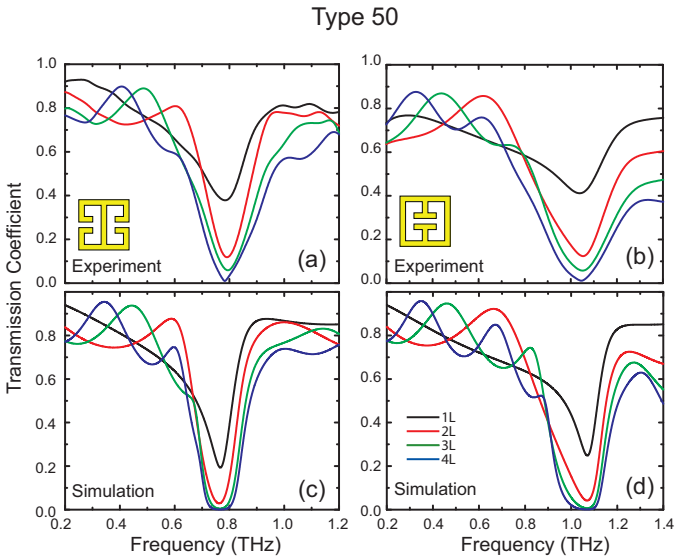

FIG. 3: Experimental and simulated transmission coefficient for Type 50 metamaterials. ERR1 is shown in (a) and (c) and ERR2 in (b) and (d).

step, the entire multilayer sample, encapsulated in polyimide, was peeled off the silicon substrate, thus yielding a free-standing metamaterial multilayer structure embedded within the host dielectric material[28].

III. SIMULATION AND EXPERIMENT

The structures were simulated with a commercial finite time domain solver, CST Microwave Studio. The metamaterial itself was modeled as lossy gold with a conductivity of $\sigma_0 = 4.56 \times 10^7$ (S/m). The embedding dielectric had a frequency independent lossy dielectric of $\widetilde{\epsilon} = 2.89 + 0.08i$. ERR1 and ERR2 are designed to have resonances at 0.76 THz and 1.07 THz, respectively. In Fig. 2 we show the dependence of the metamaterial resonance frequency, (for a single layer), on layer thickness (d) in the propagation direction, i.e. in the direction of **k** (see Fig. 1). In all cases, the metamaterial lies in the center of the dielectric layer. Dashed vertical lines at two different thicknesses show that, for both structures, the resonance frequency is continuing to change as a function of layer thickness for 15μm, but is saturated for 50μm. We simulated all sixteen metamaterial samples and performed extraction of the optical constants for each using Eq. (2). For the four layer metamaterial structure, with each layer being 50μm, the total thickness of the film is 200μm. With a resonance frequency for ERR1 (ERR2) of ω_1=0.76THz (ω_2=1.07THz), the corresponding resonant wavelength of λ_1=395 (λ_2=280) μm is comparable to its thickness.

Fabricated samples were experimentally characterized using terahertz time-domain spectroscopy (THz-TDS), which permits amplitude and phase measurements of the transmitted electric field. A reference measurement was also characterized, (open channel), thus permitting determination of absolute transmission coefficient. Experimental data for all samples and reference measurements was collected over 25ps. The complex transmission coefficient permitted us to calculate the frequency dependent dielectric function through inversion of the Fresnel equations. Etalons resulting from multiple reflections within the metamaterial were incorporated into the extraction algorithm[29,30].

IV. RESULTS

The transmitted electric field for each metamaterial ERR1 and ERR2 is shown in Fig. 3 (a) and (b) for a polyimide layer thickness of 50μm. We take the single layer ERR1 sample (black curve Fig. 3 (a)) as a point of discussion, which yields 90% transmission at 200GHz and at a frequency of 1.2 THz is about 80% transmissive. A minimum of 40% is observed at about 0.75 THz and the curve is otherwise featureless. Transmission for the other Type 50 ERR1 samples also each show minima near 0.75THz with values of 12%, 5%, and 0.1% for n=2,3, and 4 layers, respectively. Notice that, unlike the n=1 thick ERR1 transmission, other samples show oscillatory behavior beyond just the minimum near 0.75THz. For example the n=2 thick ERR1 sample (red curve), shows a local minimum of 72% at 450 GHz and a local maximum of 80% at 675 GHz. This local maximum seems to shift lower for an increase in the number of layers, i.e. 500GHz for n=3 and 425GHz for n=4 layers. This trend is also observed for the ERR2 metamaterial.

ERR1 with a 15μm thick substrate (Type 15), on the other hand, yields a transmission which does not seem to follow the same trend. For example the n=1 layer shown in Fig. 4 (a) shows a transmission minimum near 0.8

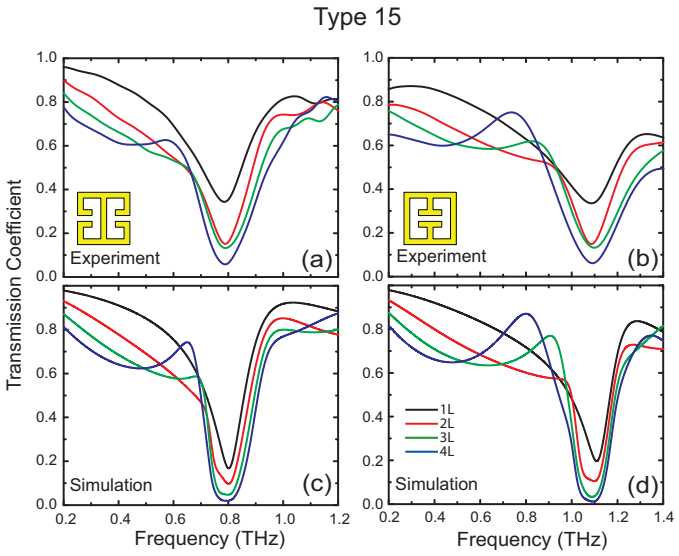

FIG. 4: Experimental and simulated transmission coefficient for Type 15 metamaterials. ERR1 is shown in (a) and (c) and ERR2 in (b) and (d).

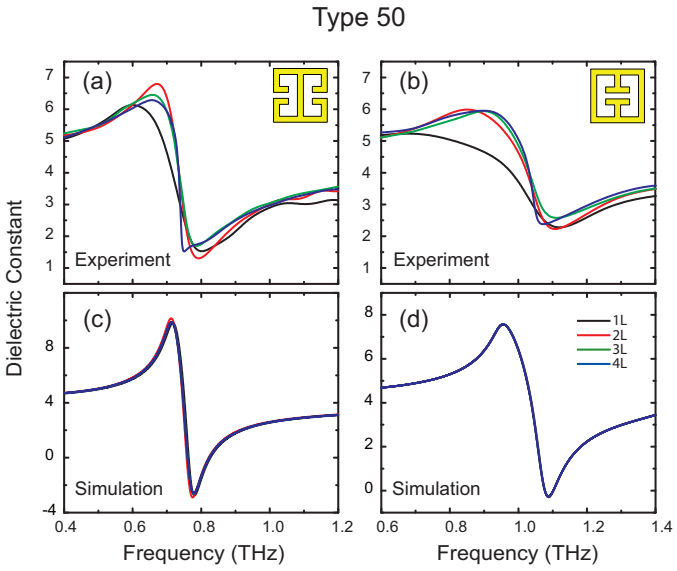

FIG. 5: Experimentally determined dielectric function for Type 50 metamaterials for ERR1 (a) and ERR2 (b). Simulated dielectric function for Type 50 results for ERR1 are shown in (c) and ERR2 in (d).

THz followed by maximum of 83% at 1.0 THz. The n=2 and n=3 layers are not so different with the maximum moving non-monotonically to 0.95 and 0.98 THz. In the n=4 sample a local minimum and maximum of 60% and 62% appear at 0.45 and 0.6THz, respectively. The 15μm thick ERR2 sample has roughly the same transmissive behavior.

In Fig. 3 (c) and (d) the simulated transmissions are shown for 50μm-thick ERR1 and ERR2, respectively. We achieve good agreement between simulated and experimental transmission, i.e. characteristic frequency dependent features discussed above for the experimental results are all observed in the simulated transmission. Although the value of transmission maxima in the experimental and computational curves is similar, there is discrepancy in the minima. For example the simulated minimum for n=1 layer thick ERR1 sample (black curve) shown in Fig. 3 (c) is 25% compared to a value of 40% for the experimental curve (black curve in Fig. 3 (a)). A similar disagreement is found for all transmission data presented in Fig. 4.

The refractive index and the impedance of each configuration can be determined from the amplitude and phase of the transmitted electric field, see Eq. 1. For the electric metamaterials studied here, the structure is composed of two combined split ring resonators with identical sizes facing either inward or outward within a single unit cell. Magnetic coupling is thus forbidden by symmetry and the electric response dominates[31,32]. We thus take the relative permeability $\mu_r = 1$ for each configuration such that the dielectric function can be obtained from Eqs. 3 and 4. Despite the periodic nature of multilayer samples, we take their total thickness to account for the relative difference in phase, (compared to a reference pulse), e.g. the phase change for a n=2 type 50 sample is calculated over 100 μm. The experimentally determined dielectric function for metamaterial samples with 50μm layer thickness are presented in Fig. 5 (a) and (b). The permittivity for ERR1 and ERR2 shows Lorentz like oscillators centered at ω_1=0.75 THz and ω_2=1.05 THz, respectively. As can be observed, there is little change in the permittivity for each sample for all layer thicknesses. There is, however, a discrepancy between the n=1 metamaterial and others for both ERR1 and ERR2.

Fig. 5 shows the simulated results for ERR1 (c) and ERR2 (d) with a substrate thickness of 50μm. Four different simulations are presented for each metamaterial, where the black, red, green, and blue curves are for n=1,2,3, and 4 layers thick, respectively, in the propagation direction. As can be observed, the extracted dielectric function for all metamaterial single and multiple layer structures are identical, with no change in oscillator strength or cental frequency location.

In order to elucidate the nature of the above results, we also simulated and characterized the dielectric function for both ERR1 and ERR2 for a different substrate embedding thickness of 15μm (Type 15). Figure 6 presents results of this investigation where (a) and (b) shows the frequency dependent permittivity for both metamaterials and (c) and (d) show the corresponding simulations. It can be observed that the permittivity is seen to change for an increasing number of layers, from one to four (black, red, green, and blue curves). Specifically, for both ERR1 and ERR2, the resonance frequency red-shifts and the maximum peak amplitude decreases for multiple lay-

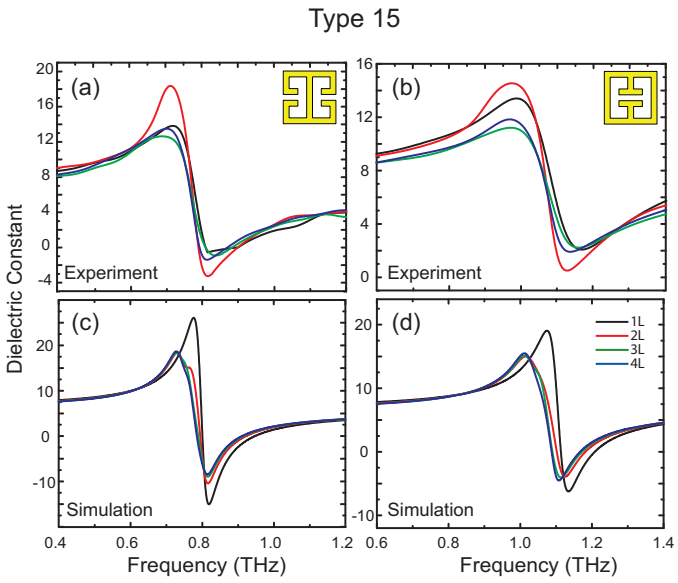

FIG. 6: Experimentally determined dielectric function for Type 15 metamaterials for ERR1 (a) and ERR2 (b). Simulated dielectric function for Type 15 results for ERR1 are shown in (c) and ERR2 in (d).

ers. Small variations in peak amplitude and peak position for each configuration are observed.

V. DISCUSSION

It is evident that the optical constants, displayed in Figs. 5 and 6, for Type 50 and Type 15 samples behave differently, although they are comprised of the exact same metamaterial geometry (for both ERR1 and ERR2). As shown in Fig. 2, the resonant frequency of these metamaterials continually shifts to lower frequencies as a function of layers thickness, until finally asymptoting around 50μm. For the 50μm-thick samples, the saturated resonance indicates that the substrate is of sufficient thickness and dielectric constant such that there is negligible interaction between adjacent metamaterial layers. This shows that the electromagnetic response within a unit cell can be treated as a homogenous response, i.e. in the effective medium limit, and is independent of the number of layers. Thus in the Type 50 case, we may define a set of optical parameters for the single layer metamaterial which is equivalent to a bulk response.

In contrast the 15μm-thick samples yield significant interaction between adjacent unit cells, owing to the relatively thin substrate and dielectric value. When stacking multiple cells, the range of the layer-to-layer coupling exceeds the unit cell thickness and neighboring unit cells interact. Unlike the previous case, it would not be correct to describe a single layer 15μm thick sample by a set of optical constants, as $\epsilon(\omega)$ depends upon the number of layers. In our studies the response seems to saturate above six layers, (not shown), for the Type 15 metamaterials.

Our computational investigations suggest that metamaterials consisting of only a single layer may or may not be describable by the optical constants ϵ and μ. This depends on some key parameters, namely the embedding dielectric thickness, the complex dielectric constant of the embedding dielectric, the filling fraction, and the particular type of metamaterial geometry, i.e. the symmetry point group and its relation to incident radiation[33]. A non-changing, layer independent, permittivity in the 50μm thick samples (Type 50) versus a gradually red-shifting permittivity in the 15μm thick samples (Type 15) is observed. Although this is clear in simulation it is apparent that there is some discrepancy for experimental measurements of single layer structures, both for Type 50 and Type 15 metamaterials. All experimental and simulated transmittance data (Fig. 3) match well, but the experimentally determined permittivities between the two cases (Type 50 and Type 15) is not as prominent as expected. This discrepancy can be attributed to the relatively weak mechanical strength of polyimide single layer films.

A thin polyimide film, although well characterized by optical constants[28], is highly flexible, mechanically weak and not self supporting. In the single layer case the as measured films surface is slightly modulated resulting in undesirable effects. We find that surface wrinkling leads to a non-uniform lattice parameter which presents itself as inhomogeneous broadening and thus a reduction in oscillator strength, (black curves in Fig. 5 (a) and (b)). In transmission this results in a lower absorptive feature and thus higher transmission. For example it can be observed that the disagreement between experimental and simulated transmission ΔT=T$_{exp}$-T$_{sim}$ (Fig. 3 and 4) is worse for single layer metamaterials but gradually improves with more layers. If we take the minimum in transmission as our point of evaluation we find ΔT=18% for single layer Type 50 films. With the addition of more metamaterial layers an increase in mechanical strength is achieved and significantly less surface fluctuations were observed in the measurements of multilayer configurations for both 15μm and 50μm structures. Indeed ΔT diminishes for n=2,3,4 layers and is 10%, 6% and 1%, respectively.

Simulated results shown for the Type 15 structures indicate that a significant red-shifting of the dielectric function occurs, due to interlayer coupling. As a result the optical constants of the 15μm thick metamaterial samples depend on the number of layers. Type 15 metamaterials achieve a more complicated and undesirable response compared to Type 50 (50μm thick) metamaterials. Although this may often be an unplanned interaction, this effect has been utilized in some cases to achieve unit cells with both electric and magnetic response[24,34–37]. Other examples include electromagnetic inducted transparency[38] and energy level hybridization[39–41]. It should be stressed that in order

TABLE I: Parameters of Lorentz oscillator fits to simulated Type 50 metamaterials.

Type 50	ERR1	ERR2
$\frac{\omega_p}{2\pi}$ (THz)	0.69	0.82
$\frac{\omega_0}{2\pi}$ (THz)	0.75	1.04
$\frac{\gamma}{2\pi}$ (THz)	0.054	0.097
ϵ_∞	3.62	3.86
n (#/m^3)	7.40×10^{8}	1.05×10^{9}
p (C·m)	4.74×10^{-16}	6.69×10^{-16}

to define optical constants for a single layer metamaterial, any interactions that may occur due to the addition of other materials in proximity to the surface should be minimized.

As the optical constants of the Type 50 single layer metamaterials explored here are *equivalent to bulk*, we may calculate the number of electric dipoles involved in the electric responses shown here. Lorentz oscillators are fit to the simulated data, shown in Figs. 5 and 6, and described by,

$$\epsilon_r(\omega) = \epsilon_\infty + \frac{\omega_p^2}{\omega_0^2 + \omega^2 - i\gamma\omega} \tag{5}$$

where ω_0 is the center frequency of the oscillator, ϵ_∞ is the dielectric constant at frequencies much greater than ω_0, γ is the damping, and ω_p^2 is the square of the plasma frequency given by,

$$\omega_p^2 = \frac{ne^2}{\epsilon_0 m}. \tag{6}$$

where n is the number density (number of charges per unit volume $n = N/V$) involved in the oscillation, e is the charge of an electron, and m is the mass of an electron.

We may also connect the number of charges (N) involved in the metamaterial resonance to the electric dipole p from assuming a form for the electric dipole moment of,

$$\mathbf{p} = -Ne\mathbf{d}. \tag{7}$$

where d is the metamaterial gap of 4μm. Table 1 lists the parameters of Lorentzian fits to the dielectric functions of Type 50 ERR1 and ERR2, including the calculated number of charges N determined from Eqs. 5 – 7 and using a volume of V=L^3 where L=50μm for Type 50 metamaterials.

As a general prescription for use of the optical constants for single layer metamaterials one may proceed as follows. First systematically explore the scattering parameters, (or effective dielectric properties - e.g. resonance frequency), of single layer metamaterials as a function of embedding dielectric thickness. Once this parameter asymptotes to a steady state solution one can be sure the fields (electric and magnetic) have diminished to the point that any material placed at the metamaterial boundary will not affect its electromagnetic properties. Thus all the microscopic details of the single layer metamaterial may be ignored and considered to be truly homogenized and well described by the optical constants.

VI. CONCLUSION

We have computationally and experimentally explored the conditions under which single layer metamaterials may be described by bulk optical constants. Two types of electric metamaterials were explored, both with two different sizes of embedding dielectric. The Type 50 configuration was a cubic unit cell with a lattice parameter of 50μm, and the Type 15 configuration was a tetragonal unit cell, with dimensions $50 \times 50 \times 15$ μm^3. The tetragonal metamaterials were shown to yield layer dependent optical constants, whereas the cubic Type 50 metamaterials yielded layer independent optical constants. A Lorentz oscillator model was fit to Type 50 metamaterials which permitted determination of the total number of charges involved in the primary metamaterial resonance.

This research was funded by the Department of Energy under DOE contract No. DE-SC0002554. We thank Mikhail Lapine for useful discussions.

[1] V. G. Veselago, Sov. Phys. Usp. **10**, 509–514 (1968).
[2] D. R. Smith, W. J. Padilla, D. C. Vier, S.C. Nemat-Nasser, and S. Schultz, Phys. Rev. Lett. **84**, 4184–4187 (2000).
[3] R. A. Shelby, D. R. Smith, and S. Schultz, Science **292**, 77–79 (2001).
[4] D. R. Smith, J. B. Pendry, and M. C. K. Wiltshire, Science **305**, 788–792 (2004).
[5] D. Schurig et al. Science **314**, 977–980 (2006).
[6] J. B. Pendry, D. Schurig, and D. R. Smith, Science **312**, 1780–1782 (2006).
[7] N. I. Landy and W. J. Padilla, Opt. Express **17**, 14872–14879 (2009).
[8] J. B. Pendry, Phys. Rev. Lett. **85**, 3996–3969 (2000).
[9] N. Fang et al. Science **308**, 534–537 (2005).
[10] E. Cubukcu, K. Aydin, E. Ozbay, S. Foteinopoulou, and C. M. Soukoulis, Phys. Rev. Lett. **91**, 207401 (2003).
[11] J. D. Jackson *Classical Electrodynamics* (John Wiley & Sons, Inc. 1999) 3rd edition.
[12] T. C. Choy, *Effective Medium Theory* (Oxford Science Publiciations, 1999).
[13] D. R. Smith and J. B. Pendry, J. Opt. Soc. Am. B-Opt. Phys. **23**, 391–403 (2006).
[14] C. R. Simovski, and S. A. Tretyakov, Phys. Rev. B **75**, 195111 (2007).
[15] C. R. Simovski, Opt. Spectrosc. 726–753 (2009).
[16] D. R. Smith, Phys. Rev. E **81** 036605 (2010).
[17] Y. Minowa et al. IEEE Trans. Terahertz Sci. Tech. Vol **1** (2011).
[18] H. Mosallasei, and K. Sarabandi, Antennas Propag. Soc. Int. Symposium IEEE 615–618 (2005).
[19] J. O'Hara, A. K. Azad, and A.J. Taylor, Eur. Phys. J. D **58**, 243–247 (2010).
[20] A. Alexopoulos, Phys. Rev. E **81**, 046607 (2010).
[21] T. Koschny, P. Markos, D. R. Smith, and C. M. Soukoulis, Phys. Rev. E **68**, 065602 (2003).
[22] D. R. Smith, D. C. Vier, Th. Koschny, and C. M. Soukoulis, Phys. Rev. E **71**, 036617 (2005).
[23] C.R. Simovski, Metamaterials **1**, 62–80 (2007).
[24] N. I. Landy, S. Sajuyigbe, J. J. Mock, D. R. Smith, and W. J. Padilla, Phys. Rev. Lett. **100**, 207402 (2008).
[25] H. Tao et al. Opt. Express **16**, 7181–7188 (2008).
[26] H. T. Chen et al. Opt. Express **15**, 1084 (2007).
[27] J. F. O'Hara et al. J. Nanoelectronics and Optoelectronics **2**, 1–6 (2007).
[28] H. Tao et al. J. Phys. D: Appl. Phys. **41**, 232004 (2008).
[29] I. Pupeza, R. Wilk, and M. Koch, Opt. Express **15**, 4335–4350 (2008).
[30] M. Scheller, C. Jansen, and M Koch, Opt. Commun. **282**, 1304–1309 (2009).
[31] D. Schurig, J. J. Mock, and D. R. Smith, Appl. Phys. Lett. **88**, 041109 (2006).
[32] W. J. Padilla et al. Phys. Rev. B **75**, 041102R (2007).
[33] W. J. Padilla, Opt. Express **15**, 1639 (2007).
[34] M. Choi et al. Nature **470**, 369 (2011).
[35] E. Tatartschuk, A. Radkovskaya, E. Shamonina, and L. Solymar, Phys. Rev. B **81**, 115110 (2010).
[36] M. Lapine et al. Appl. Phys. Lett. **95**, 084105 (2009).
[37] D. A. Powell, M. Lapine, M. V. Gorkunov, I. V. Shadrivov, and Y. S. Kivshar, Phys. Rev. B **82**, 155128 (2010).
[38] N. Liu, L. Langguth, T. Weiss, J. Kastel, M. Fleischhauer, T. Pfau, H. Giessen, Nature Mater. **8**, 758–762 (2009)
[39] J. Zhou, T. Koschny, M. Kafesaki, and C. M. Soukoulis, Phys. Rev. B **80**, 035109 (2009).
[40] N. Liu and H. Giessen, Phys. Status Solidi B **246**, 1397-1406 (2009)
[41] N. Liu and H. Giessen, Angewandte Chemie International Edition **49**, 9838–9852 (2010).